Acoustic Detection of Oceanic Double-Diffusive Convection: A Feasibility Study

TETJANA ROSS

Dalhousie University, Halifax, Nova Scotia, Canada

ANDONE LAVERY

Woods Hole Oceanographic Institution, Woods Hole, Massachusetts

(Manuscript received 3 March 2009, in final form 23 September 2009)

ABSTRACT

The feasibility of using high-frequency acoustic scattering techniques to map the extent and evolution of the diffusive regime of double-diffusive convection in the ocean is explored. A scattering model developed to describe acoustic scattering from double-diffusive interfaces in the laboratory, which accounted for much of the measured scattering in the frequency range from 200 to 600 kHz, is used in conjunction with published in situ observations of diffusive-convection interfaces to make predictions of acoustic scattering from oceanic double-diffusive interfaces. Detectable levels of acoustic scattering are predicted for a range of different locations in the world's oceans. To corroborate these results, thin acoustic layers detected near the western Antarctic Peninsula using a multifrequency acoustic backscattering system are shown to be consistent with scattering from diffusive-convection interfaces.

1. Introduction

Double-diffusive convection, an instability caused by the large difference in the molecular diffusivities of heat and salt, can create fluid layering structures stretching hundreds of kilometers (Schmitt et al. 1987; Muench et al. 1990). It is thought (e.g., Ruddick and Gargett 2003) that double-diffusive convection may be important to global ocean circulation, though it is typically not accounted for in ocean circulation models because of a lack of data on the extent, evolution, and importance of double-diffusive convections. The diffusive regime of double-diffusive convection, also called the diffusive-convection mode, occurs when there is a destabilizing temperature gradient balanced by a stabilizing salinity gradient. This regime creates very sharp (typically $<$10 cm) interfaces between the well-mixed convective layers (Schmitt 1994; Kelley et al. 2003). In addition to lakes and marginal seas (e.g., Newman 1976; Özsoy et al. 1993), diffusive convection has been observed in both the Arctic and Antarctic (e.g., Robertson et al. 1995; Timmermans et al. 2008). In fact, polar regions, with their intensely cooled and relatively fresh surface water, are particularly susceptible to diffusive convection (Kelley et al. 2003). It is likely that diffusive convection is playing its most important role in terms of influencing global ocean circulation in these polar regions. However, polar regions are relatively hard to access and, as a consequence, are typically highly undersampled. In addition, diffusive convection and other fluid structures are typically sampled using microstructure profilers, which can at best provide one profile every few minutes and are also notoriously difficult to deploy in polar regions. Rapid remote sensing techniques, such as acoustic scattering techniques, could vastly increase the amount of information that can be collected in regions with such limited access.

Recently, a series of laboratory experiments aimed at measuring, quantifying, and understanding acoustic scattering from diffusive-convection interfaces were performed in the 200–600-kHz frequency range (Lavery and Ross 2007; Ross and Lavery 2009). Although there is much variability, they show that the average returns agree well with predictions from a simple scattering model that idealizes the diffusive-convection interface as an exponential decrease from upper-layer values of sound speed and density to those in the lower layer. The goal of

Corresponding author address: Tetjana Ross, Department of Oceanography, Dalhousie University, Halifax, NS B3H 4J1, Canada.
E-mail: tetjana@dal.ca

DOI: 10.1175/2009JTECHO696.1

this paper is to use this model along with published data on diffusive-convection interfaces to investigate the feasibility of using high-frequency acoustic scattering techniques to map the extent and evolution of double-diffusive convection in situ.

This work was inspired by the acoustic observations of diffusive-convection interfaces migrating and merging in the laboratory (Ross and Lavery 2009), which resemble field data such as those in Neshyba et al. (1971), which in turn may be showing interface heaving and splitting in the Arctic. If acoustic observation of diffusive-convection interfaces in the field is possible, acoustic techniques will provide a tool for ''filling the gaps'' between sparse conductivity–temperature–depth (CTD) profiles and provide improved and continuous heat-flux estimates, perhaps leading to a better understanding of the underlying physics.

This paper is organized as follows: In section 2, an acoustic scattering model developed by Lavery and Ross (2007) to predict scattering from diffusive-convection interfaces is described. In section 3, the model is used to predict acoustic scattering from oceanic diffusive-convection interfaces using data found in the literature. Then, in section 4, acoustic, zooplankton, and microstructure data from the Antarctic, in which diffusive-convection interfaces are apparent, are presented. These data suggest that scattering from these interfaces can be observed using narrowband acoustic data.

2. A scattering model for oceanic diffusive-convection interfaces

Lavery and Ross (2007) introduced a one-dimensional multilayer weak-scattering acoustic model for backscattering from diffusive-convection interfaces. In this model, the interface is divided into many thin layers, where the sound speed and density in each layer is uniform and the sound speed and density profiles can take either idealized forms, such as an exponential or linear variation within the interface, or are obtained from measured profiles. To use measured profiles in the model, however, the profiles must be of very high resolution, resolving scales at least an order of magnitude smaller than the wavelength of sound used. When high-resolution measured profiles are not available, an idealized profile is preferable. Lavery and Ross (2007) found that, of the idealized profiles tested, the exponential profile (which when used in the multilayer acoustic model will be referred to here as the exponential model) gave the best representation of the laboratory scattering data.

In the multilayer model, the scattering from each sublayer is assumed to be weak, and thus all higher-order, multiple-scattering terms are discarded. The scattered pressure due to each subinterface is calculated and added coherently. The ratio of the amplitudes of the backscattered pressure to the incident pressure at the interface $P_{\text{scat}}/P_{\text{inc}}$ is then given by

$$\left(\frac{P_{\text{scat}}}{P_{\text{inc}}}\right) = \left[R_{\text{I},1} + \sum_{n=1}^{N} R_{n,n+1} \exp\left(2i \sum_{m=1}^{n} k_m \Delta\right)\right], \quad (1)$$

where Δ is the thickness of the homogeneous sublayers (generally chosen to be at least 20 times smaller than the wavelength of sound at the frequency of interest) and k_m is the acoustic wavenumber within the fluid sublayer m. Two additional assumptions implicit in the above formulation are that the interface thickness is much smaller than both the range to the diffusive-convection interface r (i.e., $\Delta z = N\Delta << r$) and the length of the transmitted pulse. The reflection coefficients in (1) are given by

$$R_{n,n+1} = \frac{1}{2}\left(\frac{\rho_{n+1}c_{n+1} - \rho_n c_n}{\rho_{n+1}c_{n+1} + \rho_n c_n}\right), \quad (2)$$

where ρ_n is the density and c_n is the sound speed in the sublayer n. Within the nomenclature of this model, the properties of the layer above the interfacial region (i.e., above the sublayer 1) are given by the subscript I and those of the layer below the interface (i.e., below sublayer N) are indicated by the subscript II and $R_{N,N+1} = R_{N,\text{II}}$. For the exponential model, the values of ρ_n and c_n input into (2) are calculated from

$$\begin{aligned} \rho_n &= \rho_{\text{I}} + (\rho_{\text{II}} - \rho_{\text{I}})(1 - e^{n\Delta/d_\rho}), \\ c_n &= c_{\text{I}} + (c_{\text{II}} - c_{\text{I}})(1 - e^{n\Delta/d_c}). \end{aligned} \quad (3)$$

The exponential decay constants d_ρ and d_c are obtained either by fitting exponential functions to measured profiles of density and sound speed or by using the empirical relations developed by Lavery and Ross (2007),

$$\begin{aligned} d_\rho &= \frac{\Delta z}{2.3}, \\ d_c &= \frac{\Delta z}{1.93}, \end{aligned} \quad (4)$$

where Δz is the thickness of the interface.

Thus far we know that the exponential model is a good predictor for scattering from laboratory-generated diffusive-convection interfaces. However, interfaces in the laboratory are more intense and at much shallower depths than those in the ocean, so the question remains: is it possible to use acoustics to observe diffusive-convection interfaces in situ?

The good agreement between the measured scattering from laboratory-generated diffusive-convection interfaces

and the exponential model leads us to attempt to use the exponential model to predict scattering from oceanic diffusive-convection interfaces (see section 3). However, the differences between the laboratory diffusive-convection interfaces and those typically observed in the field should be carefully considered, including such issues as the range to the interface and the strength and thickness of the interface.

Although the exponential model assumes specular reflection and thus has different range dependence than volume scattering, in order to compare returns from diffusive-convection interfaces with other sources of sound scattering in the ocean, it is useful to express it in terms of a volume scattering strength S_v (e.g., Medwin and Clay 1998, section 9.3.3). To calculate volume scattering strength, the received pressure is first squared and integrated over some time period ($\langle|p_R(t)|^2\rangle$); then, it is scaled by the similarly integrated transmitted pressure measured at range r_0 ($\langle|p_0(t)|^2\rangle$); this ratio is then corrected for the spherical spreading (i.e., $1/r^2$ each way) and absorption (i.e., $10^{-2\alpha r}$) of the acoustic waves; finally, it is divided by the volume sampled V_s to give

$$S_v = 10\log_{10}\left(\frac{\langle|p_R(t)|^2\rangle r^4 10^{\alpha r/5}}{\langle|p_0(t)|^2\rangle r_0^2 V_s}\right). \quad (5)$$

To express the scattering from diffusive-convection interfaces in terms of volume scattering strength, $\langle|p_0(t)|^2\rangle$ is taken to be the pressure incident on the interface (i.e., $\langle|p_0(t)|^2\rangle = P_{\text{inc}}^2$ for $r_0 = r$). Likewise, P_{scat} takes the place of $\langle|p_R(t)|^2\rangle$. However, because the model is for the scattered pressure at r, the absorption must be assumed to be already corrected for in the model output; thus, $\langle|p_R(t)|^2\rangle 10^{\alpha r/5} = P_{\text{scat}}^2$, and (5) becomes

$$S_v = 10\log_{10}\left(\frac{(P_{\text{scat}}/P_{\text{inc}})^2 r^2}{V_s}\right) \approx 10\log_{10}\left(\frac{(P_{\text{scat}}/P_{\text{inc}})^2}{\pi h\theta_{1/2}^2/2}\right), \quad (6)$$

where $P_{\text{scat}}/P_{\text{inc}}$ is the output from the exponential model. Both P_{scat} and P_{inc} are assumed to be constant for the time periods of their integration. The acoustic sampling volume V_s is dependent on the width of the beam and the pulse length (i.e., the pulse duration multiplied by c). In (6), V_s has been approximated as $\pi h r^2\theta_{1/2}^2/2$, which is a reasonable assumption for narrowbeam echo sounders, where h is the pulse length and $\theta_{1/2}$ is the angle (in radians) of the half beamwidth.

The model predictions $P_{\text{scat}}/P_{\text{inc}}$ are not in themselves a function of either the width of the acoustic beam or the pulse length. The model assumes a point source and is therefore summing contributions over a much wider range of angles than $\pm\theta_{1/2}$ (i.e., over an infinite number of Fresnel zones). If, however, the acoustic beam is wide enough to contain at least a few Fresnel zones, the point source assumption appears to be robust, which is suggested by both the agreement with laboratory results with only 2.5–6 Fresnel zones within the beamwidth (Lavery and Ross 2007) and by numerical integrations having shown relatively quick convergence to the infinite sum (Sheng and Hay 1993). The result is that, as long as the beam is wide enough to contain a few Fresnel zones, widening it further will not increase the scattered pressure. Also, as long as the pulse length is much longer than the interface thickness, the model predicts the same constant scattered pressure level for the duration of the pulse. As long as the integration time period is less than or equal to the pulse duration, we should get the same result regardless of pulse length. Other targets, however, will increase in number as the beamwidth and pulse length, and thus the sampling volume V_s, are increased. When attempting to resolve diffusive-convection interfaces, it is therefore advantageous to use as narrow a beam and, for narrowband signals, as short a pulse as possible.

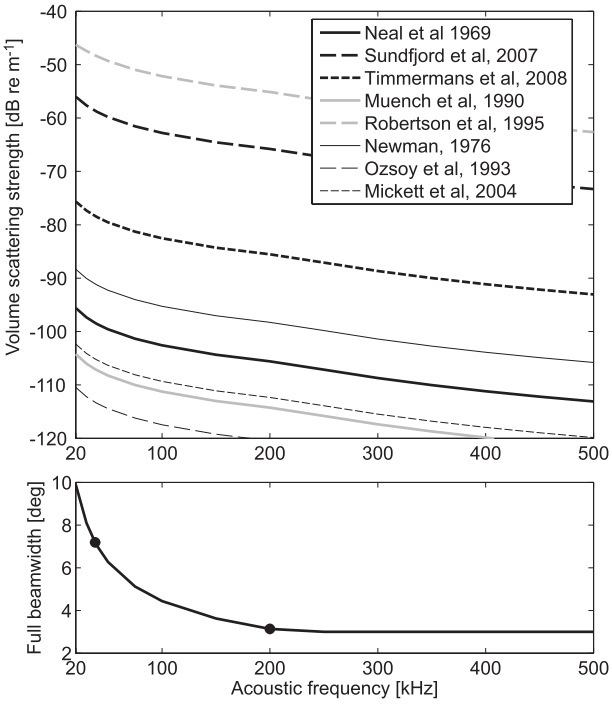

FIG. 1. (top) Estimates of the maximum in situ scattering levels for diffusive-convection interfaces as a function of acoustic frequency. The volume scattering strengths were predicted, using the exponential model, from published studies of diffusive convection (parameters are tabulated in Table 1). (bottom) A plot of the frequency-dependent full beamwidths used in the calculation of the volume scattering strengths of the diffusive-convection interfaces. The circles mark the frequencies tabulated in Table 1.

TABLE 1. Published field observations of diffusive-convection interfaces and the volume scattering strengths S_v at 38 and 200 kHz calculated using the exponential scattering model. The model assumes that the acoustic integration length scale is at least 15 cm, because shorter-integration time scales are rarely used in practice, or equal to twice the interface thickness. As in Fig. 1, the full width of the acoustic beam is assumed to be 7.2° for 38 kHz and 3.1° for 200 kHz.

Location	Depth (m)	T (°C)	ΔT (10^{-2} °C)	S (psu)	ΔS (10^{-2} psu)	Δz (m)	S_v (38 kHz) (dB re m^{-1})	S_v (200 kHz) (dB re m^{-1})
Arctic								
Neal et al. (1969)	300–340	−0.5	2.6	34.7[a]	0[a]	<0.2	>−98	>−106
Sundfjord et al. (2007)	40–75	−1	10–30	34	4–14[b]	0.05–0.1	−76 to −59	−82 to −66
Timmermans et al. (2008)	260–285	0.25–0.55	2–4	34.5–34.7	0.7–3	0.07–0.1	−90 to −78	−98 to −85
Weddell Sea								
Muench et al. (1990)[c]	100–180	−1.8 to 0.1	2–10	34.3–34.7	0.2–1	<1[d]	>−121 to >−107	>−128 to >−114
Robertson et al. (1995)	300–350	−1.0	10–50	34.6	2–4	0.02–0.3[e]	−91 to −48	−98 to −55
Lake Kivu								
Newman (1976)	200	23.0	1–3	0.0	1	0.1–0.2	−106 to −91	−113 to −98
Black Sea								
Özsoy et al. (1993	100–120	8.3–8.5	3	20.5–21.0	5	<1[d]	>−113	>−120
Admiralty Inlet								
Mickett et al. (2004)	100–110	9.5	2.6–4.5	30.15	2.2–2.4	0.5–0.75	−114 to −105	−121 to −112

[a] No salinity data were reported. A typical Arctic salinity and zero salinity step were assumed for the purposes of the calculation.
[b] No ΔS was given in the paper. The ΔS was estimated from a graph showing both temperature steps and the density ratio.
[c] Only the staircases identified by the authors as type A (in the thermocline) were used for the calculation.
[d] No Δz was estimated in the paper. For the purposes of the calculation, Δz was assumed to be less than or equal to the resolution of the CTD data.
[e] No Δz was estimated in the paper. The Δz was estimated from the reported heat flux q, assuming $q = C_p \rho \kappa_T (\Delta T/\Delta z)$, where C_p is the specific heat of the water and ρ is the mean density.

3. Applying the model to published field data

The top panel of Fig. 1 shows estimates of the maximum predicted in situ acoustic scattering levels, based on the exponential model described in the previous section, that would be observed in regions of the ocean where there are published data on diffusive-convection interfaces. In each case we have assumed that the pulse length was at least twice the interface thickness (as listed in Table 1). In cases where the interfaces were less than 7.5 cm, we assumed a pulse length of 15 cm (a pulse duration of about 100 μs). The full beamwidths $2\theta_{1/2}$ used at each frequency are plotted in the bottom panel of Fig. 1. They were chosen such that there were at least four Fresnel zones contained within the sampling volume at 20-m range and also that the full beamwidth was at least 3°. This means that the model assumptions should be satisfied at all ranges beyond 20 m and that the curve is also roughly equivalent to the smallest beamwidth transducers at a given frequency that are commercially available.

Table 1 tabulates the data from eight published studies, on which the model predictions are based. Although each study typically gives a range for the key parameters (interface thicknesses and the salinity and temperature steps across them), only the set of parameters that yielded the highest scattering level are included in Fig. 1. To see the range of predictions resulting from the full set of possible model parameters from each study, the full range of model predictions for two acoustic frequencies, 38 and 200 kHz, are tabulated in Table 1. These frequencies are commonly used for fish stock assessment and for studies involving zooplankton bioacoustics.

The biggest challenge in estimating these volume scattering strengths was the lack of published in situ interface thicknesses. Of the papers cited in Table 1, only Newman (1976); Robertson et al. (1995), Mickett et al. (2004), Sundfjord et al. (2007), and Timmermans et al. (2008) have hydrographic profiles of sufficient resolution to measure interface thicknesses. None of these, however, actually states the interface thickness. The thicknesses assigned in Table 1 are estimates based on the published figures, except for Robertson et al. (1995), which is based on published heat fluxes. Of the studies with low-resolution CTD data, Neal et al. (1969) estimated the thickness of the interface to be less than 20 cm and, for the remaining entries, the upper bound imposed by the stated resolution of the hydrographic data was

used in the calculation. Because the true interface thicknesses are likely an order of magnitude smaller, Fig. 1 and Table 1 therefore grossly underestimate the scattering from the diffusive-convection interfaces in these studies.

There is a wide range of predicted scattering strengths as well as a wide range of potential acoustic environments in which these interfaces occur. Aside from in the northern Barents Sea (Sundfjord et al. 2007), the Canada Basin (Timmermans et al. 2008), and one location in the Weddell Sea (Robertson et al. 1995), even the largest scattering predictions for frequencies above around 200 kHz are close to or below the detection limit of most sonars. In addition, based on the exponential model, the scattering at the lower frequency is predicted to be consistently higher. Combining this with the fact that a lower-frequency sonar generally has better depth penetration and less scattering contribution from zooplankton (though often more from fish), lower frequencies are likely a better choice for observing diffusive-convection interfaces in situ. However, given that the model has only been tested in the frequency range of 200–600 kHz, we restricted our calculations to frequencies close to this range.

Overall, the results in Fig. 1 and Table 1 show that, under most conditions, diffusive-convection interfaces will create measurable levels of acoustic backscattering at frequencies below approximately 40 kHz. Additionally, under some conditions, diffusive-convection interfaces create measurable levels of backscattering across a wide frequency band, thus making multifrequency observations feasible, which will increase the quality of the acoustic observations by decreasing the possibility of misidentifying layers (more on this in section 4). It appears that these conditions are most likely to occur in polar waters because the temperature steps are generally larger there. This is fortuitous because increasing the available data on diffusive convection through acoustic techniques will be most beneficial in polar regions because they are hard to access.

4. Observations of acoustic scattering from thin layers

While calibrating an acoustic system off the coast of the western Antarctic Peninsula (Fig. 2) during a Southern Ocean (SO) Global Ocean Ecosystem Dynamics (GLOBEC) cruise in 2002 (Hofmann et al. 2004; Lawson et al. 2004), high-frequency narrowband acoustic scattering and temperature/salinity microstructure data were collected in a region with two thermohaline steps (Fig. 3). Because these data were collected serendipitously, there is no information available on the history of these interfaces. There is some suggestion, from plotting temperature against salinity for the hydrographic profiles, that they were created by interleaving rather than pure double diffusion (Kelley et al. 2003). However, the microstructure data show sharp interfaces with temperature and salinity steps appropriate for diffusive-convection interfaces; thus, they should exhibit the same scattering characteristics as the laboratory interfaces, so long as the scattering is not dominated by an alternative mechanism.

Acoustic backscattering data, at 120 and 200 kHz, were collected with the Bio-Optical Multifrequency Acoustical and Physical Environmental Recorder (BIOMAPER-II; Wiebe et al. 2002a). Simultaneous microstructure and lower-resolution CTD data were collected during two casts of the CTD-Microstructure Profiling System (CMiPS; Wiebe et al. 2002b), shown as gray circles in the smallest inset of Fig. 2. The equipment and data analysis methods are described in detail in Lawson et al. (2004; acoustics) and Absy et al. (2008; microstructure). Briefly, at the time these data were collected, the BIOMAPER-II system was pinging at a rate of about 0.5 Hz on two downward-looking 120- and 200-kHz transducers. The pulse duration at both frequencies was 5 ms, and the full beamwidths were 3°. The pulses transmitted were not gated sine waves at the given frequency, but rather the frequency was slowly increased over a band of 10 kHz surrounding the target frequency, and pulse compression techniques were used to improve the signal-to-noise ratio and range resolution (Ehrenberg and Torkelson 2000). This leads to an effective pulse duration of 180 μs and a vertical resolution in the acoustic data of about 24 cm. The transducers were calibrated in situ using a 38-mm tungsten carbide calibration sphere (the sphere is visible as the continuous line between 30 and 60 m in Fig. 3), and the acoustic data were converted into volume scattering strength (Lawson et al. 2004) on a ping-by-ping basis. The BIOMAPER-II also records environmental variables (such as temperature, pressure, etc.), and the pressure data were used to plot the acoustic data at the correct depth (the acoustic system was initially towed at about 16-m depth, then was lowered in steps to about 30 m). The CMiPS collected microtemperature and microconductivity data using two FP07 thermistors and a SeaBird SBE 7 microconductivity sensor. Additionally, high-resolution pressure was sampled. All high-resolution data were sampled at 512 Hz. The profiles were calibrated by regressing them on the lower-resolution but higher-precision CTD data.

Figure 3 shows that acoustic scattering layers were observed at the locations of the thermohaline steps observed with the CMiPS. The upper interfacial scattering layer is at about 100-m depth, and the lower interfacial scattering layer is between 120 and 130 m. The scattering layers are more prominent at 120 than at 200 kHz. This

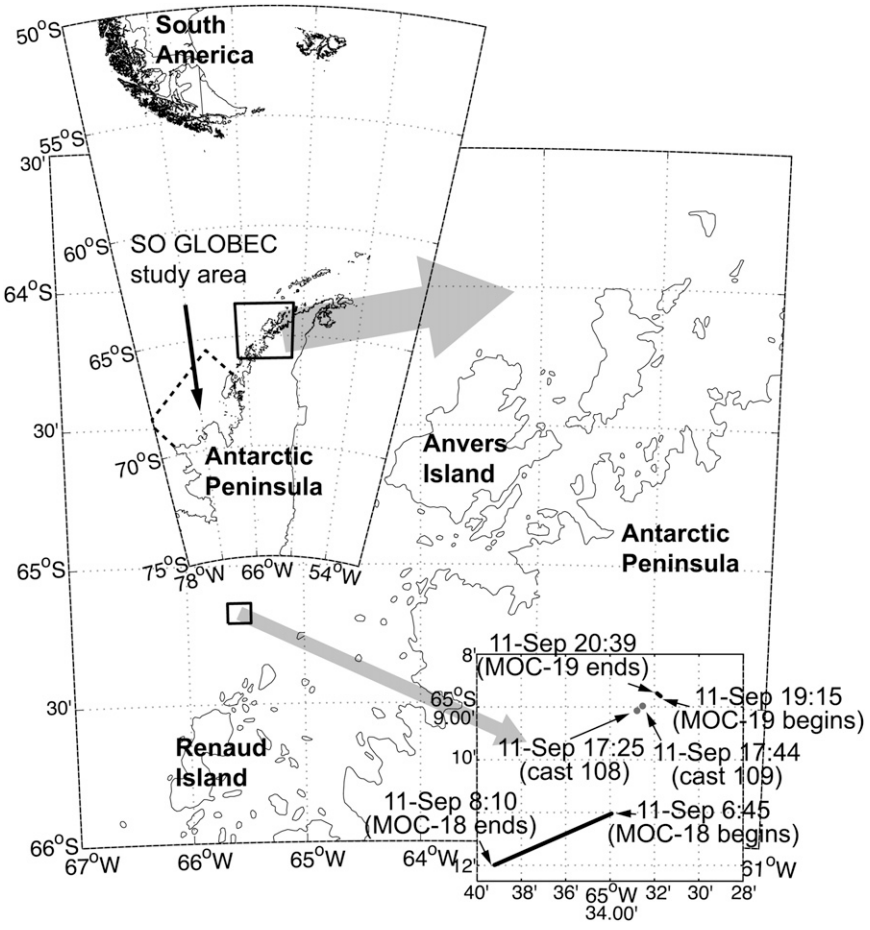

FIG. 2. The 2002 data collection site: all times are local (UTC − 4 h).

is in part due to the lower noise level, but, as the exponential model would predict, the volume scattering was also stronger at the lower frequency. This can be seen in the bottom panel of Fig. 3. The layer thickness was determined for each ping by stepping out one depth bin at a time from the depth of the peak S_v in the layer and only retaining those depths that maintained S_v above a threshold (−96 dB for 120 kHz and −94 dB for the noisier 200 kHz). This could result in anywhere from 1 to 20 depth bins being considered interfacial scattering. However, the interfacial layer was rarely thicker than 12 bins (3 m). All the interfacial points that had been retained in the above procedure for 10 consecutive pings were then averaged. All averages of scattering strength were computed in linear space and then converted into decibels for plotting. The background scattering level was estimated by taking the average of the scattering strength just above and below the depth range of the interfacial scattering layer (again, anywhere from 1 to 20 bins, because they were the remaining bins from a 5.25-m-depth range surrounding the layer maximum). Although quite variable, the 10-ping mean volume scattering strength in the upper interfacial layer is generally higher at 120 kHz than at 200 kHz, except when the strength of the interfacial layers are weak enough so that the 200-kHz data are influenced by the background scattering strength (i.e., when the confidence intervals of the mean layer and the mean background volume scattering strength overlap). The variability seen in the scattering strength of the interfacial layer is consistent with the large amount of variability (on scales from 2 s to 10 min) seen in laboratory scattering experiments (Lavery and Ross 2007).

Figure 4 shows the predicted and measured volume scattering strengths from the in situ data for the upper interface. The high-resolution temperature and salinity profiles shown in Fig. 3 were used to calculate sound speed (shown in Fig. 4, top) and density profiles, and then each interface was fit with an exponential, (4), to calculate ρ_{I}, ρ_{II}, d_ρ, c_{I}, c_{II}, and d_c, which were then input into the exponential model. For comparison, the same was done for the linear model discussed in Lavery and

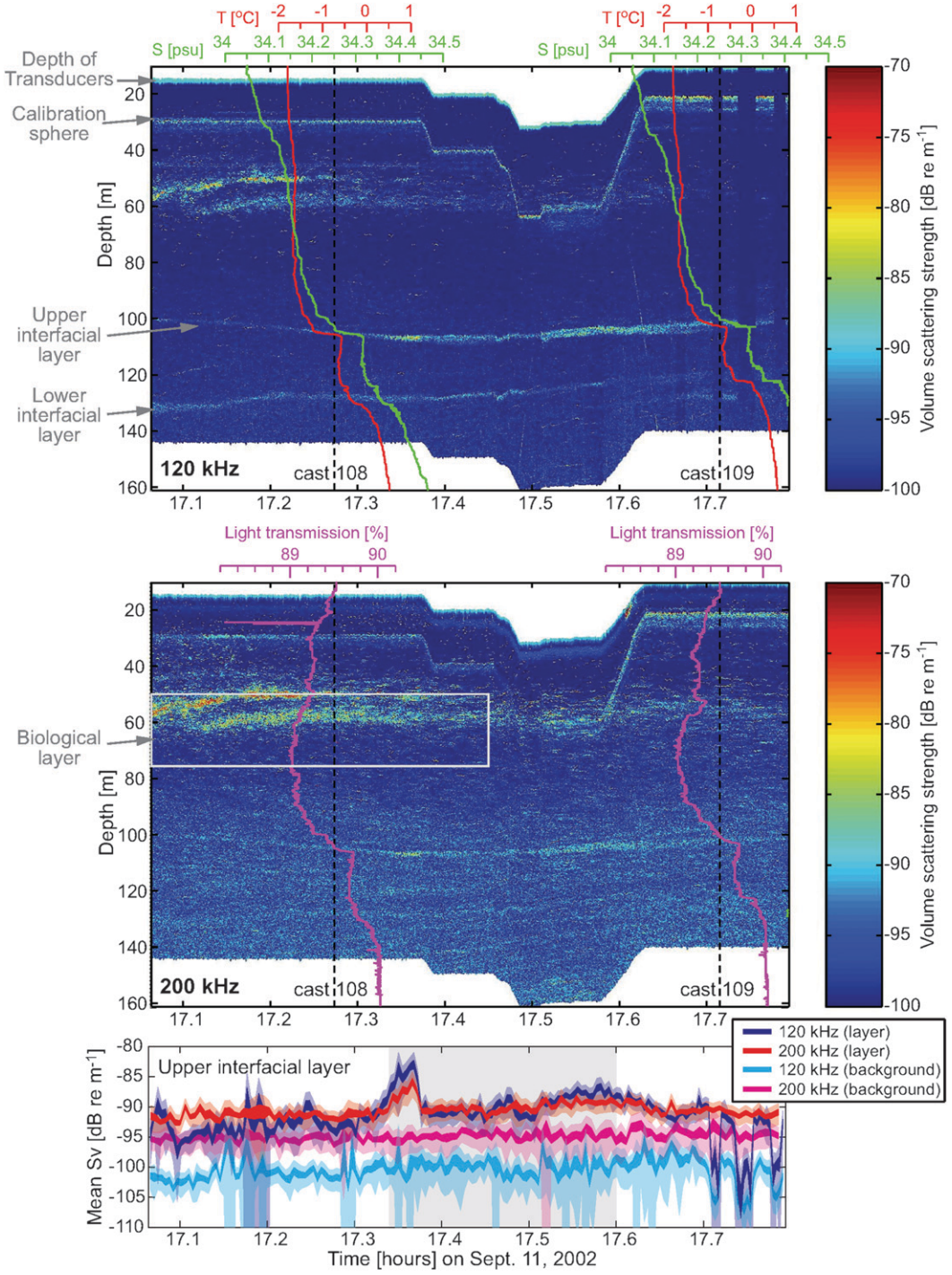

FIG. 3. Echograms collected with BIOMAPER II (top) 120- and (middle) 200-kHz downward-facing transducers. Overlaying the echograms are (top) temperature and salinity and (middle) transmissometer profiles collected simultaneously with the acoustic data. (bottom) The 10-ping-averaged S_v in the upper interfacial layer at both 120 and 200 kHz, as well as the background scattering levels, is shown. The thickness of the dark lines indicates the standard error in the means, whereas the lighter shaded areas indicate the 99.9% confidence intervals. The light gray box indicates the time period where the 200-kHz layer scattering was significantly different than background. All times are local (UTC − 4 h).

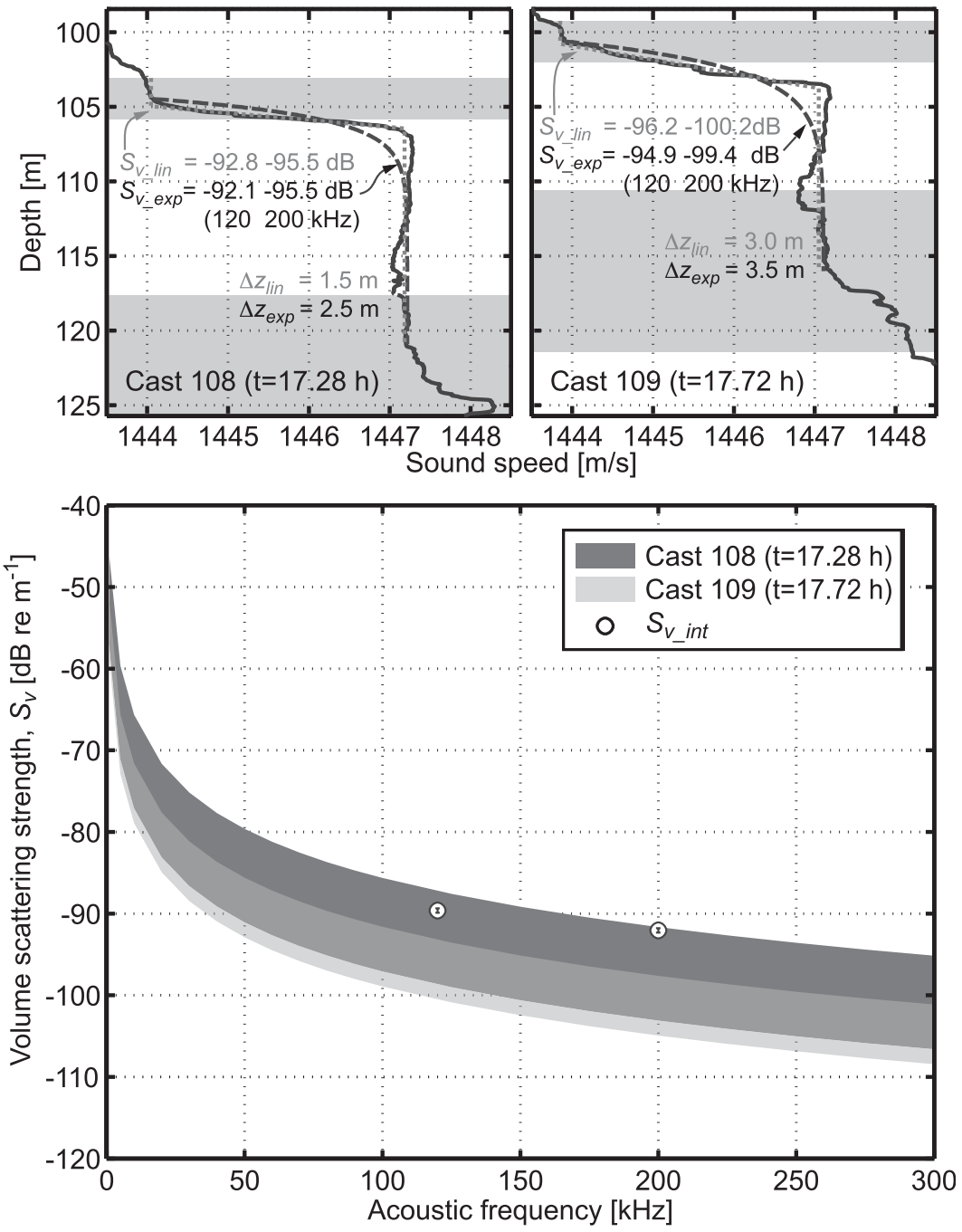

FIG. 4. (top) Sound speed profiles: (left) cast 108 and (right) cast 109. The dashed black lines show the exponential fit to the interface for the midpoint of the range of starting points (shown as gray boxes) used in the bootstrapped fit. The dotted gray line shows a linear fit to the interface. The equivalent interface thicknesses Δz and the results of applying the diffusive-convection scattering model to each fit and averaging over 10 kHz are indicated. (bottom) Comparison between scattering levels predicted using the exponential model and the in situ observations of the upper scattering layer in Fig. 3. The bounded areas show the bootstrapped 95% confidence intervals (Efron and Gong 1983) for the model output based on fitting exponentials to the upper step in the two profiles. The circles are the background-noise-corrected average volume scattering strengths for the upper interfacial layer across all the data shown in Fig. 3, and the error bars are 99.9% confidence intervals (i.e., 3.39se, where se is the standard error).

Ross (2007). This is shown with the gray dotted line in the top panels of Fig. 4. A 10-kHz average of the predicted scattering strengths from both models based on the profiles shown are indicated in the figure. The two models yield similar results.

Because the in situ profiles show much more variability than those from the laboratory experiments on which the model is based, the biggest uncertainty in the estimation of S_v came from the depth window chosen to isolate the interface for the exponential fit. Thus, the bootstrap 95% confidence intervals (Efron and Gong 1983) shown as shaded regions in the upper panels of Fig. 4 were calculated by simultaneously and randomly varying both ends of the depth window (within a reasonable range, i.e., still ensuring that data clearly unrelated to the interface were not included). The lower interface was weaker and not as sharp and therefore less well defined in the profiles. This increased uncertainty in the model output to the point that comparison with the measured scattering was not informative and is therefore not displayed.

The in situ volume scattering strengths (the symbols in Fig. 4) are averaged over the depth of the first interfacial scattering layer, using data for all times shown in Fig. 3. The S_v values plotted in Fig. 4 are the noise-corrected average volume scattering strengths for the 120- and 200-kHz sounders. Assuming the background scattering is unrelated to the diffusive-convection interface and is likely also present at the depth of the interface, this should give the best representation of the scattering from the interface.

Although the density and sound speed steps are one to several orders of magnitude smaller in the in situ data than in the laboratory experiment, the exponential model predicts observable intensities for the volume scattering strength. Indeed, the predicted S_v for profile 108 agrees with the observed intensities of the upper interfacial scattering layer at both 120 and 200 kHz, and the prediction based on profile 109 is within 3–5 dB. The decrease in the noise-corrected interfacial scattering strength from 120 to 200 kHz is 2.4 ± 0.2 dB re m^{-1}. This is just over half the 4.5 dB re m^{-1} decrease in the model predictions.

Other sources of acoustic scattering

The observed agreement between predicted and observed volume scattering strengths in the interfacial scattering layer does not, in itself, prove that the scattering was caused by the diffusive-convection interfaces. However, other data collected as part of the project show that the two other likely sources of scattering in the interfacial region are unlikely to have caused the observed patterns.

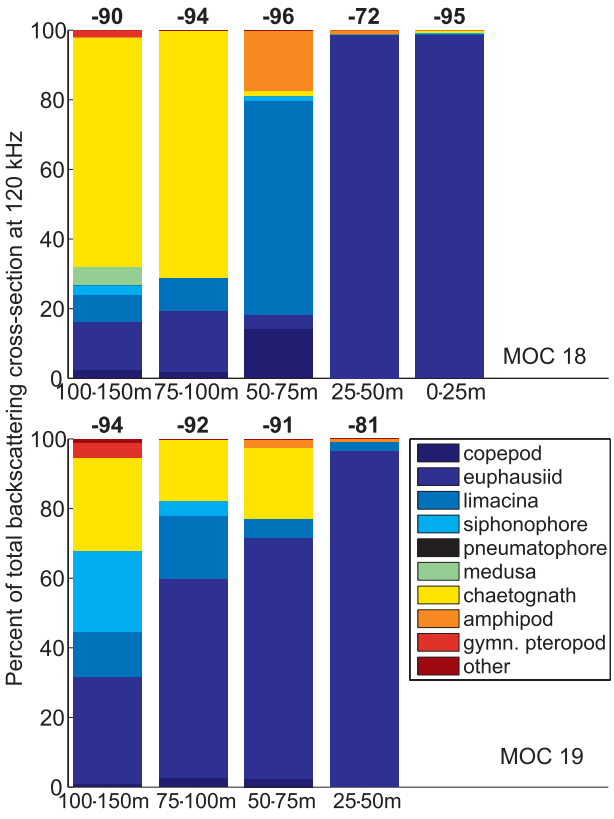

FIG. 5. Zooplankton scattering models applied to all MOCNESS data. The size of the colored bars indicates the relative scattering contribution of a particular taxon at 120 kHz. The numbers atop each set of bars indicates the total estimated volume scattering strength for that net in dB re m^{-1}.

1) ZOOPLANKTON

There was no shortage of zooplankton in the region (Wiebe et al. 2002b). Thus, it is possible that a zooplankton layer coincident with the thermohaline steps could have caused the interfacial scattering layer. Although no plankton net data were collected coincident with the acoustic/CMiPS data discussed here, there was one daytime 1 m^2 Multiple Opening/Closing Net and Environmental Sensing System (MOCNESS) tow conducted in the region about 10 h before (MOC-18) and another about 2 h later (MOC-19; see Fig. 2), after dark. Zooplankton scattering models, as described in Lawson et al. (2004, 2006), were applied to the analyzed contents of the nets (Fig. 5).

In Fig. 6, the top panel focuses on the nets that sampled the 100–150-m-depth range and the bottom panel focuses on the 50–75-m-depth range, showing the predicted total spectra for both tows. Note that, although Fig. 5 shows that the scattering was dominated by different groups, the scattering levels are not too different and the trend for higher scattering strength at higher

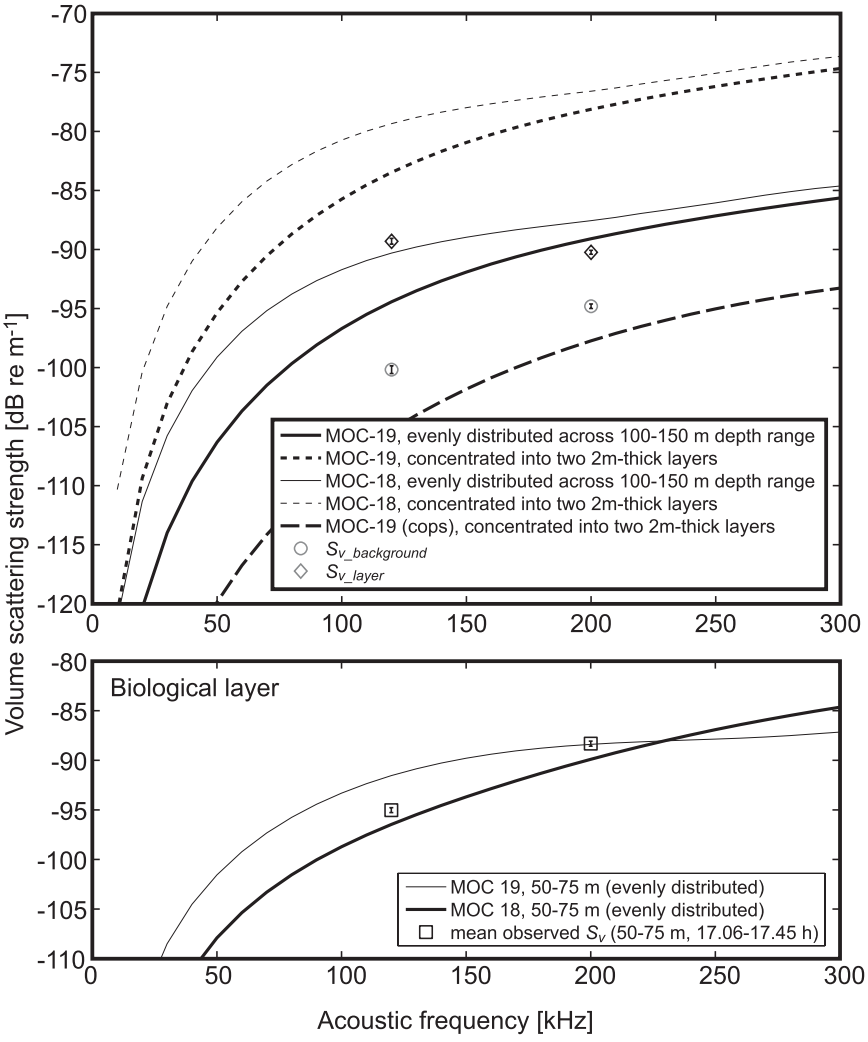

FIG. 6. Comparison between scattering levels predicted from zooplankton scattering models based on the contents of the nets that sampled the (top) 100–150- and (bottom) 50–75-m-depth ranges at two different locations near to where the acoustic data were collected (see Fig. 2) and the observed scattering levels. (top) The scattering levels both in the upper interfacial layer $S_{v\text{-layer}}$ and immediately surrounding it $S_{v\text{-background}}$ are shown. (bottom) The mean scattering level throughout the 50–75-m-depth range is shown. The error bars are 99.9% confidence intervals (i.e., 3.39se, where se is the standard error).

frequencies is present in all nets. Also, although the lines plotted here do not show the true uncertainties associated with the parameterization of the zooplankton scattering models (likely around 5 dB), the upward trends are fairly robust across parameterizations. Although neither net is likely truly representative of the relative abundances of organisms where and when the acoustic data were collected, that there is some agreement between day and night nets collected a couple nautical miles apart suggests that they can give us an idea of the likely trends in the biological scattering at the site.

Figure 6 also shows the mean observed volume scattering strength in the upper interfacial layer S_{v_layer} as well as the mean volume scattering strength immediately surrounding the interfacial scattering layer $S_{v\_\text{background}}$. Note that the difference between the backscattering cross sections (σ, where $S_v = 10\log_{10}\sigma$) associated with these were plotted in Fig. 4 [i.e., $S_{v\_\text{int}} = 10\log_{10}(\sigma_{\text{layer}} - \sigma_{\text{background}})$, where $S_{v\_\text{layer}} = 10\log_{10}(\sigma_{\text{layer}})$ and $S_{v\_\text{background}} = 10\log_{10}(\sigma_{\text{background}})$].

There were enough zooplankton present that, if they were all aggregated into two 2-m-thick layers coincident with the thermohaline steps (dashed lines; Fig. 6), they would cause a level of scatter stronger than what was observed. However, scattering from these organisms cannot explain the slight decrease in the volume scattering

strength of the interfacial layer with increasing acoustic frequency. The observed decrease with frequency of the total volume scattering strength in the interfacial layer is modest but significant, 0.9 ± 0.2 dB re m^{-1} [95% confidence interval (CI)] in Fig. 6. It increases a little, to 1.3 ± 0.3 dB re m^{-1} (95% CI) if only data collected between 17.34 and 17.6 h are averaged. This is the time period, indicated by the gray box in the bottom panel of Fig. 3, that excludes data where the scattering at 200 kHz from the interfacial layer was not significantly different than the background (as defined by overlap in the 99.9% confidence intervals of the 10-ping means of the background and layer scattering).

A decrease in backscattering strength with frequency is typically associated with physical scattering sources (Warren et al. 2003). Although the backscattering spectra of some organisms can decrease with frequency (e.g., small gas-bearing zooplankton, but only over a restricted range of frequencies; Lavery et al. 2007), there is no evidence from either of the net tows that these organisms substantially contributed to the total zooplankton backscattering contribution (see Fig. 5). Both tows show that volume scattering strength should be higher at 200 kHz than at 120 kHz. Consequently, it seems most plausible that the animals are distributed more or less evenly throughout the water column (solid lines; Fig. 6) and that the background noise (circles; Fig. 6) is, at least in part, higher at 200 kHz because of increased biological scattering.

In the bottom panel of Fig. 6, a similar comparison between the predicted scattering based on the MOCNESS nets and the acoustic observations is performed for the net sampling the 50–75-m-depth stratum. The scattering observed at these depths is much more consistent with being of biological origin. Again, the zooplankton models predict an increase in volume scattering strength with increasing frequency. This increase is also seen in the observed volume scattering strength; the squares in the bottom panel of Fig. 6 are the mean volume scattering strength in the light gray box indicated in Fig. 3 (note that, although the box is slightly offset from the center of the acoustic scattering layer, it exactly corresponds to the depth stratum of the MOCNESS net). Here, the observations agree better with the predictions from MOC-18, which was collected 10 h before the acoustic data. This may be because the acoustic data were collected just before sundown and the animals at that depth could be diel migrators, or it may be explained by the inherently patchy nature of in situ zooplankton distributions.

Both MOC-18 and MOC-19 showed that copepods smaller than 2.5 mm were numerically dominant and also a large contributor to the total scattering at many depths (Fig. 5). These small animals, being relatively weak swimmers, are the most likely to be passive acoustic tracers of physical processes. However, the predicted frequency dependence for scattering by copepods increases with increasing frequency (see dashed line on Fig. 6); despite their numbers, they were a relatively small component of the total zooplankton backscattering contribution for the 100–150-m-depth range. In addition, there is further independent support from the transmissometer data collected with the CTD (Fig. 3, middle), which show no evidence of an increased particle load at the location of the interfaces. The transmissometer, sampling at 24 Hz and falling at about 0.6 m s^{-1}, collected 40–80 samples within the 1–2-m-thick scattering layer. If the copepods were concentrated on the interfaces, then, based on the approximate volume sampled by the transmissometer, the transmissometer data are expected to show at least one spike as it passed through the interfaces. This spike would have an amplitude of about 1% (Beardsley et al. 1996) and would look like the spike seen at about 25 m in the first cast. Thus, although there is some evidence in the transmissometer data of an increased particle load in the upper water column, there is nothing that supports an aggregation of small zooplankton on the interfaces.

In summary, predictions of volume scattering strength based on two zooplankton net tows collected in the vicinity of the interfaces, approximately 12 h apart and under different light conditions (day/night), increase with increasing frequency. The measured scattering from the interfacial layer, however, showed the opposite trend, suggesting that it is not of biological origin. Additionally, transmissometer data, collected contemporaneously with the acoustic data, also suggest that there was no aggregation of small copepods in the interfacial layer.

2) MECHANICAL TURBULENCE

Another possible source of the interfacial scattering is turbulence caused by shear on the interface (Batchelor 1957; Ross and Lueck 2003; Warren et al. 2003). Scattering from turbulent microstructure could explain the decrease in intensity with increasing acoustic frequency (Warren et al. 2003). There is, however, no reason to believe that there is significant shear on the interfaces, which could lead to enhanced turbulence. Although no velocity data are available, there appears to be no forcing in the region to cause shear and mixing on those deep interfaces. Dissipation rates, estimated by fitting Batchelor spectra to the CMiPS temperature microstructure data, as shown in Fig. 7 (Kocsis et al. 1999), are quite low, except right in the interfaces. Because the Batchelor fits were generally poor in the interfacial regions, the dissipation rates estimated in the surrounding waters, $O(10^{-9}$ W $kg^{-1})$, are probably a better representation

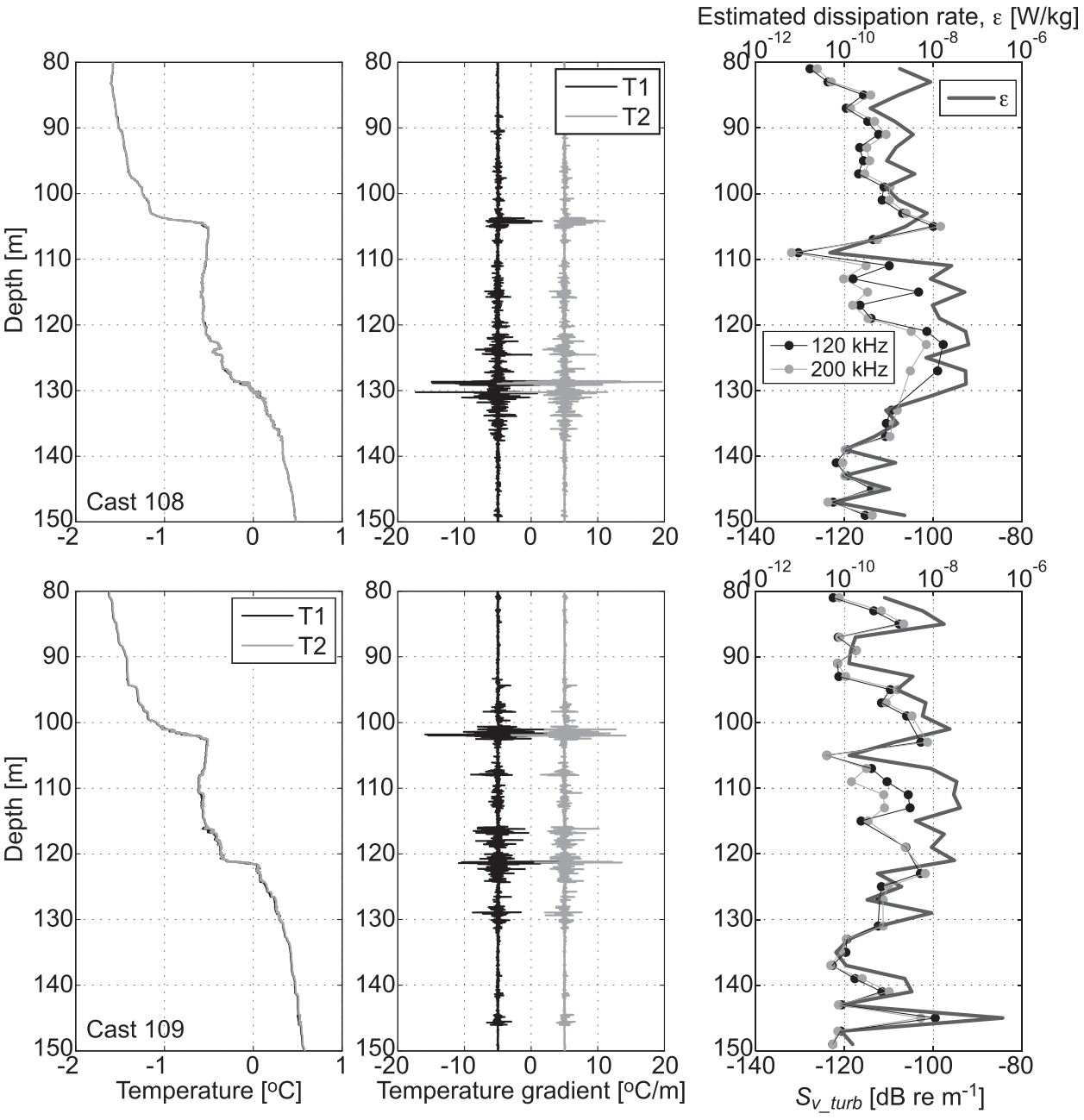

FIG. 7. The CMiPS temperature microstructure data for profiles 108 and 109 are shown: (left) the temperature profiles, highlighting the location of the interfaces; (middle) the microscale vertical temperature gradient offset to improve clarity, and (right) the dissipation rates estimated by fitting Batchelor spectra to temperature spectra calculated from 2-m segments of temperature gradient data. Also plotted is the predicted volume scattering strength at 120 and 200 kHz, based on a turbulence scattering model.

of the true dissipation rates in the interfaces. A turbulence scattering model was applied (Ross and Lueck 2005), using the estimated dissipation rates and the mean temperature and salinity gradients over the same 2-m segment, to estimate the scattering contribution from turbulence. The results are shown in Fig. 7 [depths where the Batchelor fits were very poor (i.e., where the integral of the variance under the measured spectrum and the fitted spectrum differed by more than a factor of 2) are not plotted]. The predicted volume backscattering rarely exceeds -100 dB re m^{-1}, even at the lower frequency, and these higher values only occur in the region of the interfaces, where the dissipation rates were likely overestimated. Thus, the predicted turbulent scattering

contribution is generally well below the levels predicted for diffusive-convection interfaces, which suggests that the temperature microstructure is caused by some other mechanism, such as double diffusion.

5. Summary and discussion

This study illustrates how acoustics can be used to identify and monitor diffusive-convection interfaces in the ocean. A simple scattering model based on idealized sound speed and density profiles that makes use of published data on diffusive-convection interfaces predicts that these interfaces will scatter sound at measurable levels in many regions in the ocean: with typical field equipment, with typical in situ thermohaline step sizes, and at typical depths of occurrence. The SO GLOBEC data suggest that diffusive-convection interfaces have already, inadvertently, been observed acoustically off the western Antarctic Peninsula.

Acoustic observation of double-diffusive layers is highly complimentary to traditional microstructure or hydrographic measurements. The speed (typically one acoustic profile per second) and ease (no extra manpower) with which acoustics can sample the water column allows the observation of high-frequency variability missed by profiles. Proper acoustic characterization of the scattering from diffusive-convection interfaces has the double benefit of potentially improving acoustic estimates of zooplankton biomass (e.g., Warren and Wiebe 2008).

Additionally, by employing broadband acoustic techniques (Stanton and Chu 2008; Chu and Stanton 1998) in their laboratory experiments, Lavery and Ross (2007) and Ross and Lavery (2009) showed that the centimeter-scale interface thicknesses can be continuously and remotely measured, the evolution and migration of the interfaces can be observed, and the speed of the convective cells in the adjacent well-mixed layers can be estimated. Ross and Lavery (2009) further show that the acoustically estimated interface thicknesses, combined with coarse-resolution temperature measurements, allow direct estimates of conductive heat fluxes across the interfaces. Extension of these broadband techniques to the field could lead to even more information on double-diffusive processes being gained.

Increasing the number and richness of observations could prove to be a key element in addressing questions of the importance of diffusive convection in global ocean circulation, especially because most of the regions susceptible to diffusive convection are polar. There are fewer sampling opportunities in polar regions because of the need for expensive ice breakers, increasing the benefit of a speedier measurement technology. Understanding the role of double diffusion in the Arctic is particularly pressing. Because of the recent decreases in summer ice extent, more ice is melting and forming each year, increasing the thermohaline forcing, which triggers changes in the diffusive-convection staircases and potentially their role in the system.

Acknowledgments. Many thanks to the researchers in the Southern Ocean GLOBEC project for sharing their data and their time, most notably Peter Wiebe and Gareth Lawson (BIOMAPER-II), Laurie Padman (CMiPS), and Bob Beardsley (transmissometer). We are grateful to Max Li, a Woods Hole Oceanographic Institution (WHOI) Summer Student Fellow, who did the preliminary analysis of the Antarctic data, including the analysis of the MOCNESS net tows and some initial acoustic analysis. TR is grateful to the Natural Sciences and Engineering Research Council of Canada Discovery Grant and University Faculty Award Programs, which support her work at Dalhousie University.

REFERENCES

Absy, J., M. Schröder, R. Muench, and H. H. Hellmer, 2008: Early summer thermohaline characteristics and mixing in the western Weddell Sea. *Deep-Sea Res. II,* **55,** 1117–1131.

Batchelor, G. K., 1957: Wave scattering due to turbulence. *Proc. Symp. on Naval Hydrodynamics,* Washington, DC, National Academy of Sciences, 409–423.

Beardsley, R. C., A. W. Epstein, C. Chen, K. F. Wishner, M. C. Macaulay, and R. D. Kenney, 1996: Spatial variability in zooplankton abundance near feeding right whales in the Great South Channel. *Deep-Sea Res. II,* **43,** 1601–1625.

Chu, D., and T. Stanton, 1998: Application of pulse compression techniques to broadband acoustic scattering by live individual zooplankton. *J. Acoust. Soc. Amer.,* **104,** 39–55.

Efron, B., and G. Gong, 1983: A leisurely look at the bootstrap, the jacknife, and cross-validation. *Amer. Stat.,* **37,** 36–48.

Ehrenberg, J. E., and T. C. Torkelson, 2000: FM slide (chirp) signals: A technique for significantly improving the signal-to-noise performance in hydroacoustic assessment systems. *Fish. Res.,* **47,** 193–199.

Hofmann, E. E., P. H. Wiebe, D. P. Costa, and J. J. Torres, 2004: An overview of the Southern Ocean Global Ocean Ecosystems Dynamics program. *Deep-Sea Res. II,* **51,** 1921–1924.

Kelley, D., H. Fernando, A. Gargett, J. Tanny, and E. Ozsoy, 2003: The diffusive regime of double-diffusive convection. *Prog. Oceanogr.,* **56,** 461–481.

Kocsis, O., H. Prandke, A. Stips, A. Simon, and A. Wüest, 1999: Comparison of dissipation of turbulent kinetic energy determined from shear and temperature microstructure. *J. Mar. Syst.,* **21,** 67–84.

Lavery, A., and T. Ross, 2007: Acoustic scattering from double-diffusive microstructure. *J. Acoust. Soc. Amer.,* **122,** 1449–1462.

——, P. H. Wiebe, T. K. Stanton, G. L. Lawson, M. C. Benfield, and N. J. Copley, 2007: Determining dominant scatterers of sound in mixed zooplankton populations. *J. Acoust. Soc. Amer.,* **122,** 3304–3326.

Lawson, G. L., P. H. Wiebe, C. J. Ashjian, S. M. Gallager, C. S. Davis, and J. D. Warren, 2004: Acoustically-inferred zooplankton distribution in relation to hydrography west of the Antarctic Peninsula. *Deep-Sea Res. II,* **51,** 2041–2072.

——, ——, ——, D. Chu, and T. K. Stanton, 2006: Improved parameterization of Antarctic krill target strength models. *J. Acoust. Soc. Amer.,* **119,** 232–242.

Medwin, H., and C. S. Clay, 1998: *Fundamentals of Acoustical Oceanography*. Academic Press, 712 pp.

Mickett, J. B., M. C. Gregg, and H. E. Seim, 2004: Direct measurements of diapycnal mixing in a fjord reach—Puget Sound's main basin. *Estuarine Coastal Shelf Sci.,* **59,** 539–558.

Muench, R. D., H. J. S. Fernando, and G. R. Stegen, 1990: Temperature and salinity staircases in the northwestern Weddell Sea. *J. Phys. Oceanogr.,* **20,** 295–306.

Neal, V. T., S. Neshyba, and W. Denner, 1969: Thermal stratification in the Arctic Ocean. *Science,* **166,** 373–374.

Neshyba, S., V. Neal, and W. Denner, 1971: Temperature and conductivity measurements under ice island T-3. *J. Geophys. Res.,* **76,** 8107–8120.

Newman, F. C., 1976: Temperature steps in Lake Kivu: A bottom heated saline lake. *J. Phys. Oceanogr.,* **6,** 157–163.

Özsoy, E., Ü. Ünlüata, and Z. Top, 1993: The evolution of Mediterranean water in the Black Sea: Interior mixing and material transport by double diffusive intrusions. *Prog. Oceanogr.,* **31,** 275–320.

Robertson, R., L. Padman, and M. D. Levine, 1995: Fine structure, microstructure, and vertical mixing processes in the upper ocean in the western Weddell Sea. *J. Geophys. Res.,* **100** (C9), 18 517–18 535.

Ross, T., and R. Lueck, 2003: Sound scattering from oceanic turbulence. *Geophys. Res. Lett.,* **30,** 1343, doi:10.1029/2002GL016733.

——, and ——, 2005: Estimating turbulent dissipation rates from acoustic backscatter. *Deep-Sea Res. I,* **52,** 2353–2365.

——, and A. Lavery, 2009: Laboratory observations of double-diffusive convection using high-frequency broadband acoustics. *Exp. Fluids,* **46,** 355–364.

Ruddick, B., and A. E. Gargett, 2003: Oceanic double-infusion: Introduction. *Prog. Oceanogr.,* **56,** 381–393.

Schmitt, R. W., 1994: Double diffusion in oceanography. *Annu. Rev. Fluid Mech.,* **26,** 255–285.

——, H. Perkins, J. D. Boyd, and M. C. Stalcup, 1987: C-SALT: An investigation of the thermohaline staircase in the western tropical North Atlantic. *Deep-Sea Res.,* **34,** 1655–1665.

Sheng, J., and A. E. Hay, 1993: Spherical wave backscatter from straight cylinders: Thin-wire standard targets. *J. Acoust. Soc. Amer.,* **94,** 2756–2765.

Stanton, T. K., and D. Chu, 2008: Calibration of broadband active acoustic systems using a single standard spherical target. *J. Acoust. Soc. Amer.,* **124,** 128–136.

Sundfjord, A., I. Fer, Y. Kasajima, and H. Svendsen, 2007: Observations of turbulent mixing and hydrography in the marginal ice zone of the Barents Sea. *J. Geophys. Res.,* **112,** C05008, doi:10.1029/2006JC003524.

Timmermans, M.-L., J. Toole, R. Krishfield, and P. Winsor, 2008: Ice-Tethered Profiler observations of the double-diffusive staircase in the Canada Basin thermocline. *J. Geophys. Res.,* **113,** C00A02, doi:10.1029/2008JC004829.

Warren, J. D., and P. H. Wiebe, 2008: Accounting for biological and physical sources of acoustic backscatter improves estimates of zooplankton biomass. *Can. J. Fish. Aquat. Sci.,* **56,** 1321–1333.

——, T. K. Stanton, P. H. Wiebe, and H. E. Seim, 2003: Inference of biological and physical parameters in an internal wave using multiple-frequency, acoustic-scattering data. *ICES J. Mar. Sci.,* **60,** 1033–1046.

Wiebe, P., T. Stanton, C. Greene, M. Benfield, H. Sosik, T. Austin, J. Warren, and T. Hammar, 2002a: BIOMAPER-II: An integrated instrument platform for coupled biological and physical measurements in coastal and oceanic regimes. *IEEE J. Oceanic Eng.,* **27,** 700–716.

——, and Coauthors, 2002b: Report of RVIB *Nathaniel B. Palmer* Cruise NBP02-04 to the western Antarctic Peninsula 31 July to 18 September 2002. United States Southern Ocean Global Ocean Ecosystems Dynamics Program Tech. Rep. 8, 161 pp.